Original Article | Cardiovascular Imaging

eISSN 2005-8330
https://doi.org/10.3348/kjr.2023.0173
Korean J Radiol 2023;24(7):647-659

Korean Journal of Radiology
KJR

Correct Closure of the Left Atrial Appendage Reduces Stagnant Blood Flow and the Risk of Thrombus Formation: A Proof-of-Concept Experimental Study Using 4D Flow Magnetic Resonance Imaging

Min Jae Cha[1]*, Don-Gwan An[2,3]*, Minsoo Kang[2,3], Hyue Mee Kim[4], Sang-Wook Kim[4], Iksung Cho[5], Joonhwa Hong[6], Hyewon Choi[1], Jee-Hyun Cho[7], Seung Yong Shin[3,4], Simon Song[2,3,8]

[1]Department of Radiology, Chung-Ang University Hospital, Chung-Ang University College of Medicine, Seoul, Korea
[2]Department of Mechanical Convergence Engineering, Hanyang University, Seoul, Korea
[3]Center for Precision Medicine Platform Based-on Smart Hemo-Dynamic Index, Seoul, Korea
[4]Division of Cardiology, Department of Internal Medicine, Chung-Ang University Hospital, Chung-Ang University College of Medicine, Seoul, Korea
[5]Division of Cardiology, Department of Internal Medicine, Yonsei University College of Medicine, Yonsei University Health System, Seoul, Korea
[6]Department of Thoracic and Cardiovascular Surgery, Chung-Ang University Hospital, Chung-Ang University College of Medicine, Seoul, Korea
[7]Bio-Chemical Analysis Team, Korea Basic Science Institute, Cheongju, Korea
[8]Institute of Nano Science and Technology, Hanyang University, Seoul, Korea

Objective: The study was conducted to investigate the effect of correct occlusion of the left atrial appendage (LAA) on intracardiac blood flow and thrombus formation in patients with atrial fibrillation (AF) using four-dimensional (4D) flow magnetic resonance imaging (MRI) and three-dimensional (3D)-printed phantoms.

Materials and Methods: Three life-sized 3D-printed left atrium (LA) phantoms, including a pre-occlusion (i.e., before the occlusion procedure) model and correctly and incorrectly occluded post-procedural models, were constructed based on cardiac computed tomography images from an 86-year-old male with long-standing persistent AF. A custom-made closed-loop flow circuit was set up, and pulsatile simulated pulmonary venous flow was delivered by a pump. 4D flow MRI was performed using a 3T scanner, and the images were analyzed using MATLAB-based software (R2020b; Mathworks). Flow metrics associated with blood stasis and thrombogenicity, such as the volume of stasis defined by the velocity threshold ($|\vec{V}|$ < 3 cm/s), surface-and-time-averaged wall shear stress (WSS), and endothelial cell activation potential (ECAP), were analyzed and compared among the three LA phantom models.

Results: Different spatial distributions, orientations, and magnitudes of LA flow were directly visualized within the three LA phantoms using 4D flow MRI. The time-averaged volume and its ratio to the corresponding entire volume of LA flow stasis were consistently reduced in the correctly occluded model (70.82 mL and 39.0%, respectively), followed by the incorrectly occluded (73.17 mL and 39.0%, respectively) and pre-occlusion (79.11 mL and 39.7%, respectively) models. The surface-and-time-averaged WSS and ECAP were also lowest in the correctly occluded model (0.048 Pa and 4.004 Pa^{-1}, respectively), followed by the incorrectly occluded (0.059 Pa and 4.792 Pa^{-1}, respectively) and pre-occlusion (0.072 Pa and 5.861 Pa^{-1}, respectively) models.

Received: November 23, 2022 **Revised:** April 6, 2023 **Accepted:** April 17, 2023
*These authors contributed equally to this work.
Corresponding author: Seung Yong Shin, MD, PhD, Division of Cardiology, Department of Internal Medicine, Chung-Ang University Hospital, Chung-Ang University College of Medicine, 102 Heukseok-ro, Dongjak-gu, Seoul 06973, Korea.
• E-mail: theshin04@cau.ac.kr; and
Simon Song, PhD, Department of Mechanical Convergence Engineering, Hanyang University, 222 Wangsimni-ro, Seongdong-gu, Seoul 04763, Korea.
• E-mail: simonsong@hanyang.ac.kr

Conclusion: These findings suggest that a correctly occluded LAA leads to the greatest reduction in LA flow stasis and thrombogenicity, presenting a tentative procedural goal to maximize clinical benefits in patients with AF.
Keywords: Atrial fibrillation; Left atrial appendage occlusion; Hemodynamics; 4D flow MRI; Stasis; Thrombogenicity

INTRODUCTION

Atrial fibrillation (AF) is the most common cardiac arrhythmia and one of the leading causes of thromboembolic events such as stroke and vascular dementia [1,2]. In this pathological condition, an enlarged and fibrillating left atrium (LA) or left atrial appendages (LAAs) serve as niduses of thrombus formation in more than 90% of cases [3]; thus, most patients with AF and stroke risk are managed via oral anticoagulant (OAC) therapy [4]. However, patients who cannot tolerate long-term OAC therapy or those with a large thrombotic burden require local therapy such as LAA mechanical exclusion either by surgical excision or percutaneous closure device implantation [5,6]. Previous clinical trials, such as PROTECT-AF, PREVAIL, and PRAGUE-17, have demonstrated that percutaneous LAA occlusion (LAAO) is non-inferior to OAC therapy in preventing stroke and cardiovascular death in patients with AF [7-9].

Theoretically, the mechanical exclusion of LAAs from the LA reduces the LA chamber size and makes the chamber more spherical, thereby reducing the risk of local thrombus formation. However, there is limited information on the changes in LA hemodynamics—such as velocity, flow pattern, and stasis—that occur before and after LAAO. In addition, there is little evidence regarding the optimal closure plane for LAAO. Strokes may occur, and device-related thrombi may develop in some patients even after a successful LAAO [10,11]; therefore, a comprehensive understanding of LA hemodynamics is essential for a deeper understanding of the LAAO procedure itself and for optimal patient selection and postprocedural antithrombotic management.

In clinical practice, flow characteristics are usually evaluated using two-dimensional transesophageal echocardiography [12]. However, given the complex three-dimensional (3D) nature of the fluid dynamics within an enlarged LA, full investigation of flow using conventional two-dimensional imaging techniques is challenging. Four-dimensional (4D) flow magnetic resonance imaging (MRI) is an option for the direct visualization and characterization of 3D flow, as 4D flow MRI can assess detailed LA flow patterns in patients with AF [13-16].

We defined correct occlusion as complete closure at the plane of the LAA ostium and hypothesized that LA flow characteristics would improve after LAAO and differ between correctly and incorrectly occluded LAAs. To achieve high spatial and temporal resolutions using 4D flow MRI, in vitro experiments were planned using patient-specific, life-sized, 3D-printed LAs. In this experimental study, we aimed to investigate the effect of correct LAAO on intracardiac blood flow and thrombus formation in patients with AF using atrial 4D flow MRI and 3D-printed LA phantoms.

MATERIALS AND METHODS

The Institutional Review Board of Chung-Ang University (IRB No. 2012-003-403) approved this prospective study, and written informed consent was obtained from the participant before the initiation of the study.

Pre-Occlusion Computed Tomography (CT) in a Patient with AF

An 86-year-old male with long-standing persistent AF and a history of cerebral infarction and subdural hemorrhage participated in this study. Before LAAO, multiphasic CT (IQon Spectral CT; Philips Healthcare) was performed with retrospective electrocardiogram gating (see Supplementary Materials for the detailed CT acquisition parameters). The patient subsequently underwent LAAO, and an experienced interventional cardiologist (SYS) successfully implanted an Amplatzer Cardiac Plug (ACP) (Abbott Vascular).

Construction of LA Phantoms

Pre-occlusion CT images were imported and loaded into MATLAB software (R2020b; Mathworks) using a Digital Imaging and Communications in Medicine file format. The target LA blood pool was segmented to create a sculpture and 3D model using a standard tessellation language file format. LA endocardial surface geometry was reconstructed using the isosurface function. The final pre-occlusion LA model was created by offsetting the boundary with a 2-mm outward thickness to represent the LA wall. The model

https://doi.org/10.3348/kjr.2023.0173

Korean Journal of Radiology
KJR

was printed using a stereolithography apparatus (SLA800; ProtoFab) with a clear polycarbonate-like resin material and resolution of 0.1 x 0.1 x 0.1 mm.

To create post-occlusion LA models, ex vivo LAAO was performed by an experienced interventional cardiologist (SYS) using a model of the same size as the implanted ACP (Fig. 1). After successful LAAO of the pre-occlusion 3D-printed model, a CT scan was performed. To minimize the metal artifacts induced by the LAAO device and prevent any impact on magnetic resonance (MR) signal acquisition and 4D flow image data, we performed 3D modelling via CT prior to performing MRI. Correct LAAO was defined as the complete exclusion of the LAA at the LAA ostial plane, without any pouch remnants (Fig. 1). To create an incorrectly occluded model with a remnant pouch, the ACP was intentionally implanted at an inappropriate angle and landing zone, and CT was subsequently performed. Based on the CT images of the correctly and incorrectly occluded LA phantoms, two postprocedural LA phantoms were 3D-printed in the same manner as the pre-occlusion phantom. In total, three life-sized LA phantoms—pre-occlusion, correctly occluded, and incorrectly occluded—were produced (Figs. 1, 2). A bioprosthetic mitral valve (stented porcine mitral valve, Epic 27 mm, E100-27M; Abbott Laboratories) was installed in the three phantoms to reproduce LA flow conditions.

Patient-Specific Flow Simulation Setup

A custom-made, closed-loop flow circuit was set up (Fig. 3), comprising four flowmeters (LS-10LPM-D; Alicat Scientific, Inc.), four proportional solenoid valves (Type 2875; Bürkert), an acrylic reservoir, one pump (PP2-50Y; Hwarang System), and a data acquisition instrument (NI USB-6361; NI), to simultaneously collect real-time flow rate data and deliver patient-specific pulse signals to the pump system. The patient-specific pulmonary venous pulse was generated based on the spectral Doppler waves from four pulmonary veins (right superior, right inferior, left superior, and left inferior) obtained using transesophageal echocardiography. A high-pressure spiral hose was used to minimize the hose elasticity effects on the pulsating flow transmission. A 6 mM/L aqueous solution of copper sulfate mixed with glycerine (viscosity: 0.004 Pa·s; density: 1100 kg/m^3) at a deionized water-to-glycerin volume ratio of 3:2 was used as the working fluid to reflect the viscosity and density of human blood flow.

4D Flow MRI Acquisition

A 3-tesla MRI scanner (Achieva TX; Philips Healthcare) was used with a 32-channel SENSE head coil; detailed MR acquisition parameters are shown in the Supplementary Table 1. A time-resolved 3D three-component velocity field was obtained by subtracting the MRI phase data acquired during pump-off from those acquired during pump-on to

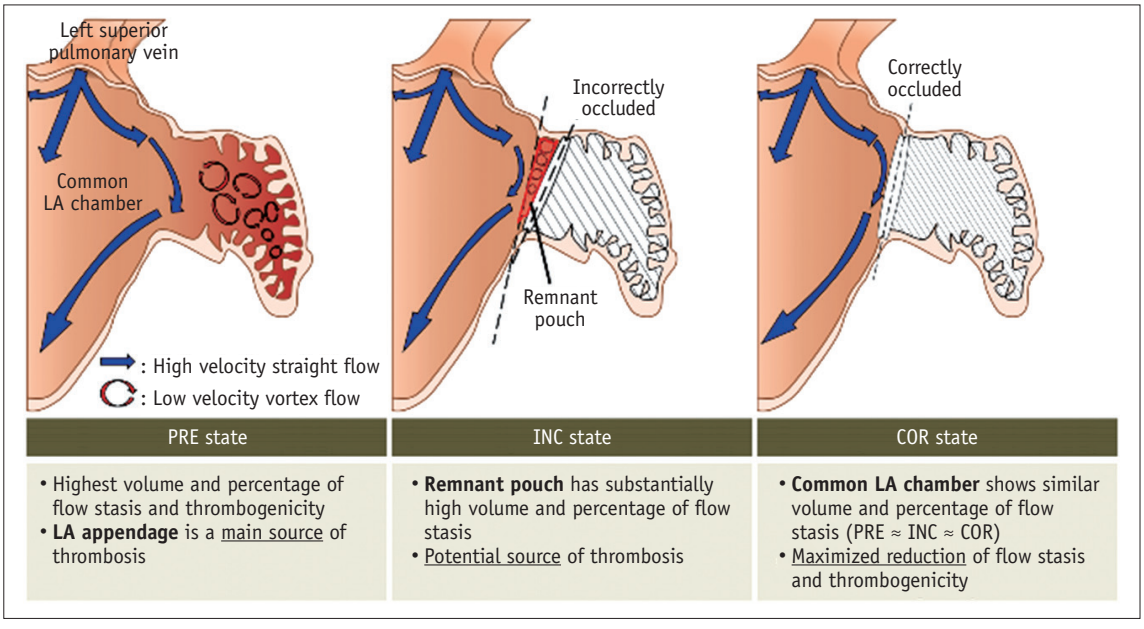

Fig. 1. Graphical illustration of pre-occlusion (PRE), incorrectly occluded (INC), and correctly occluded (COR) left atrium (LA) phantoms and summarized results of the hemodynamic analysis using 4D flow magnetic resonance imaging (MRI). The potential source of thrombosis is reduced by left atrial appendage occlusion (LAAO), and more in COR state than in INC state.

https://doi.org/10.3348/kjr.2023.0173

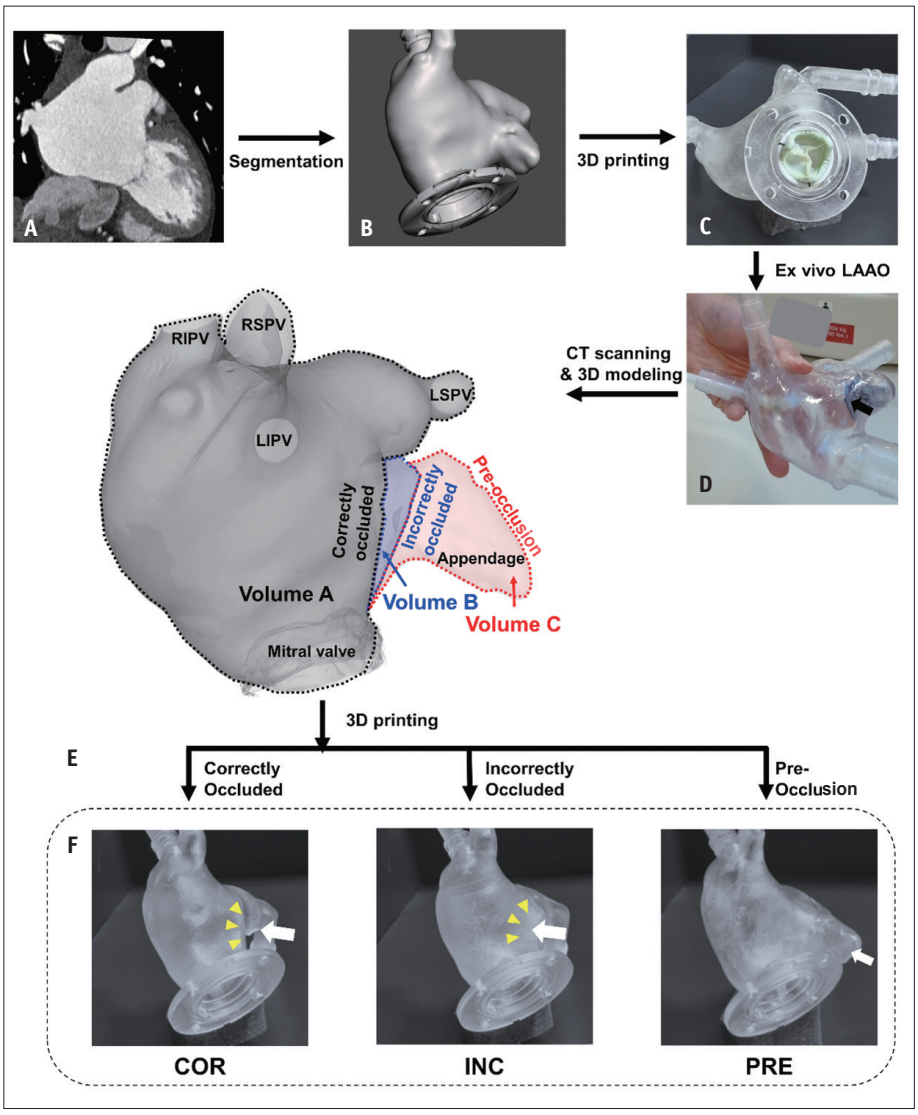

Fig. 2. Process of producing three life-sized 3D-printed phantoms of the left atrium (LA). **A:** Computed tomography (CT) image of the LA of the target patient. **B:** 3D image of the LA was reconstructed based on preprocedural cardiac CT images. **C:** 3D LA phantom was printed based on the image (pre-occlusion [PRE]). **D:** Ex vivo left atrial appendage occlusion (LAAO) was performed accurately and intentionally imprecisely in a PRE 3D LA phantom, arrow shows blockage of the appendage with the occluder. **E:** Internal volume comparison based on LAAO conditions, arrows show the internal volume changes caused by the occluder. **F:** 3D models of the correctly- and incorrectly occluded LA phantoms were printed based on the images, yellow arrowheads and white arrows indicate geometric differences near the appendage due to the occluder. RSPV = right superior pulmonary vein, RIPV = right inferior pulmonary vein, LIPV = left inferior pulmonary vein, LSPV = left superior pulmonary vein, INC = incorrectly occluded, COR = correctly occluded

compensate for the intrinsic MRI measurement errors arising from eddy currents or systems [17,18]. Additionally, because the 4D flow velocity field obtained using MRI included noise, a wall-bound divergence-free smoothing filter was applied to smooth the velocity vectors while satisfying the mass conservation law and no-slip conditions [18,19].

4D Flow MRI Data Analysis

LA flow visualization was performed using the particle traces and path lines released from the entire segmented LA volume. For each voxel inside the segmented LA, LA stasis was defined as a voxel with an absolute velocity below a threshold of 3 cm/s. The time-averaged volume of stasis during the cardiac cycle was calculated for the three different LA phantoms. Additionally, we calculated the relative amount of flow stasis, r_{stasis} (%), as proposed by Markl et al. [13]. r_{stasis} was defined as the ratio of the number of time frames with velocities below 3 cm/s (n_{stasis}) to the total number of cardiac time frames (N_{total}), for each voxel inside the LA. The particle residence time (PRT) was defined as the time taken for each

https://doi.org/10.3348/kjr.2023.0173

Korean Journal of Radiology
KJR

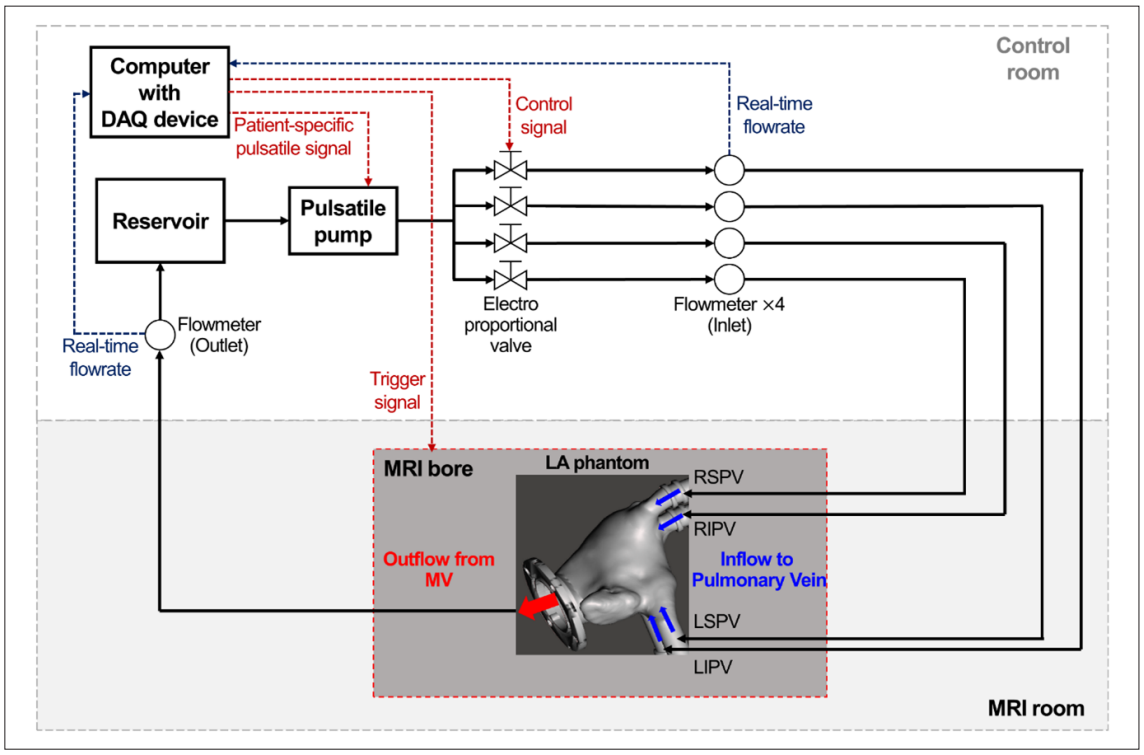

Fig. 3. Schematic of the closed-loop flow circuit. A custom closed-loop flow circuit was developed to simulate and collect the data of patient-specific blood flow using specialized equipment and magnetic resonance imaging (MRI). The red and blue arrows at the bottom center of the figure indicate the direction of flow exiting and entering the phantom, respectively. DAQ = data acquisition, LA = left atrium, RSPV = right superior pulmonary vein, RIPV = right inferior pulmonary vein, LIPV = left inferior pulmonary vein, LSPV = left superior pulmonary vein, MV = mitral valve

Table 1. Summary of Hemodynamic Parameters and Their Clinical Implications

Parameters	Definition	Equation	Clinical Implications
Wall shear stress	Viscous shear forces of flowing blood acting tangentially with respect to the LA surface		Low WSS can lead to the accumulation of blood cells and fibrin, increasing the likelihood of thrombus formation
Time-averaged wall shear stress	Time-averaged, blood-flow, shear stress acting on the LA surface over a cardiac cycle	$TA\|WSS\| = \frac{1}{T}\int_0^T \|WSS\| dt$	Low WSS can lead to the accumulation of blood cells and fibrin, increasing the likelihood of thrombus formation
Oscillatory shear index	How often the wall shear stress vector changes its direction during a cardiac cycle on the LA surface	$OSI = \frac{1}{2}\left(1 - \frac{\left\|\int_0^T WSS dt\right\|}{\int_0^T \|WSS\| dt)}\right)$	High OSI can lead to the disturbance of flow pattern, increasing the likelihood of thrombus formation
Endothelial cell activation potential	Ratio of OSI to normalized TA|WSS|	$ECAP = \frac{OSI}{TA\|WSS\|}$	High ECAP can promote platelet adhesion and aggregation, increasing the likelihood of thrombus formation
Relative amount of flow stasis	Ratio of the number of time frames with velocities below the threshold to the total number of cardiac time frames for each voxel	$r_{stasis} = \frac{n_{stasis}}{N_{total}} \times 100\ (\%)$	High r_{stasis} is associated with increased risk of thrombogenicity

LA = left atrium, WSS = wall shear stress, TA|WSS| = time-averaged wall shear stress, OSI = oscillatory shear index, ECAP = endothelial cell activation potential

https://doi.org/10.3348/kjr.2023.0173

virtual blood particle to leave the LA from an initial position, and the volume covered by the iso-PRT surface was calculated with the PRT set to five cardiac cycles. The time-to-leave the LA for the blood particle inside the iso-PRT surface was more than five cardiac cycles. We evaluated hemodynamic parameters such as the oscillatory shear index (OSI), time-averaged wall shear stress (WSS), and surface-and-time-averaged WSS [20,21].

The WSS on the LA wall was calculated using the following steps: First, an isosurface composed of small triangular cells was created using the threshold for the 4D flow MRI signal magnitude. The threshold was carefully determined such that the isosurface represented the LA wall boundary and optimally separated the fluids from the rest. Second, the strain rate tensor in the small triangular cells was computed. The velocity gradient tensors at each voxel were computed using forward or backward difference methods, depending on the voxel position. The strain rate tensor at the vertices of the triangular cells was then calculated using the cubic spline interpolation method on the velocity gradient tensor in the surrounding 125 (5 x 5 x 5) voxels. As the final step, the WSS was defined as the tangential component of the strain rate tensor to the wall, multiplied by the dynamic viscosity of the fluid. Further detailed calculations of the WSS have been described by Ko et al. [22] and Yang et al. [23]. The endothelial cell activation potential (ECAP), defined as the ratio of OSI to the normalized time-averaged absolute WSS (TA|WSS|), was also analyzed [24]. The calculation methods and clinical implications of the 4D flow MRI parameters are summarized in Table 1.

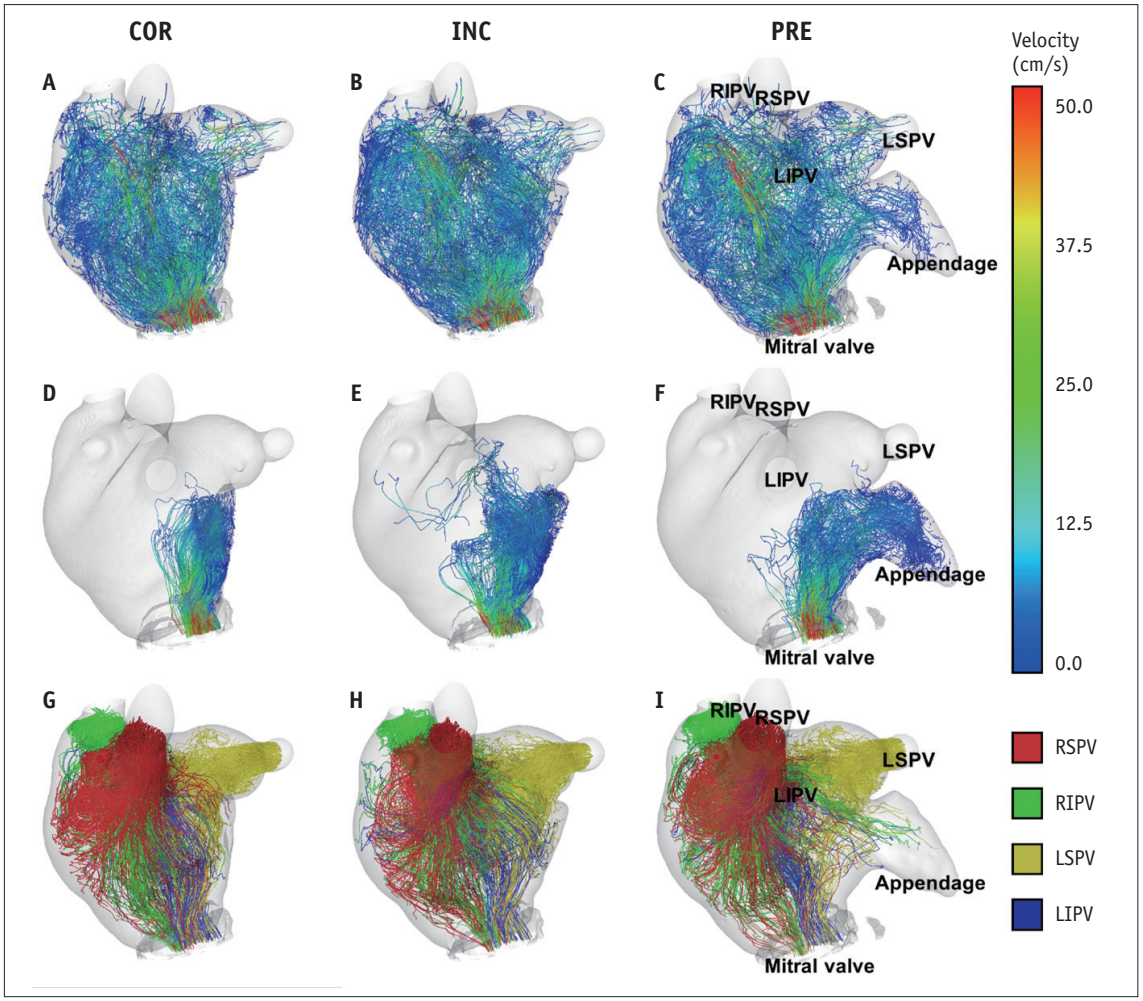

Fig. 4. Path line analysis of 4D flow magnetic resonance imaging among correctly occluded (COR), incorrectly occluded (INC), and pre-occlusion (PRE) left atrium (LA) phantoms. **A-C:** Color-coded path lines for the entire LA. **D-F:** Color-coded path lines for the region near the appendage. **G-I:** Path lines originating from the right superior pulmonary vein (RSPV) (red), right inferior pulmonary vein (RIPV) (green), left superior pulmonary vein (LSPV) (yellow), and left inferior pulmonary vein (LIPV) (blue). Each LA phantom showed a different flow pattern in terms of distribution, orientation, and magnitude.

https://doi.org/10.3348/kjr.2023.0173

Korean Journal of Radiology
KJR

RESULTS

Flow Analysis for the Three LA Phantoms

For qualitative visualization of the 4D flow MRI data, a 3D particle trace was used (Fig. 4, Supplementary Video 1). It compared the path lines of the three LA phantoms, defined by tracing hypothetical blood particle movements during cardiac cycles, and showed the various spatial distributions and orientations of the velocity vectors. Aside from the qualitative comparison, the results of the 4D flow MRI enabled direct visualization of the different 3D blood flow patterns—in terms of distribution, orientation, and magnitude—that resulted from the different LA shapes and volumes.

Comparison of LA Flow Stasis Volumes

Figure 5 shows the flow stasis volumes of the three LA phantoms. The volume of stasis, defined as the region with a velocity vector of less than 3 cm/s, was consistently the lowest throughout the entire cardiac cycle in the correctly occluded model, followed by the incorrectly occluded and pre-occlusion models. Even using different velocity thresholds for defining flow stasis, ranging from 3 cm/s to 5 cm/s, the time-averaged stasis volume was consistently the lowest in the correctly occluded model, followed by the incorrectly occluded and pre-occlusion models.

LA stasis volumes under various conditions were compared among the three phantoms (Table 2). The phantom volumes were 181.72 mL, 187.54 mL, and 199.21 mL, and the time-averaged LA stasis volumes were 70.82 mL (39.0% of the LA phantom volume), 73.17 mL (39.0%), and 79.11 mL (39.7%) for correctly occluded, incorrectly occluded, and pre-occlusion models, respectively. The LA stasis volume, calculated under different cutoff values for the persistence of stasis (r_{stasis}), was also consistently the lowest in the correctly occluded model, followed by the incorrectly occluded and pre-occlusion models. When analyzing the volume within the common LA chamber, excluding the

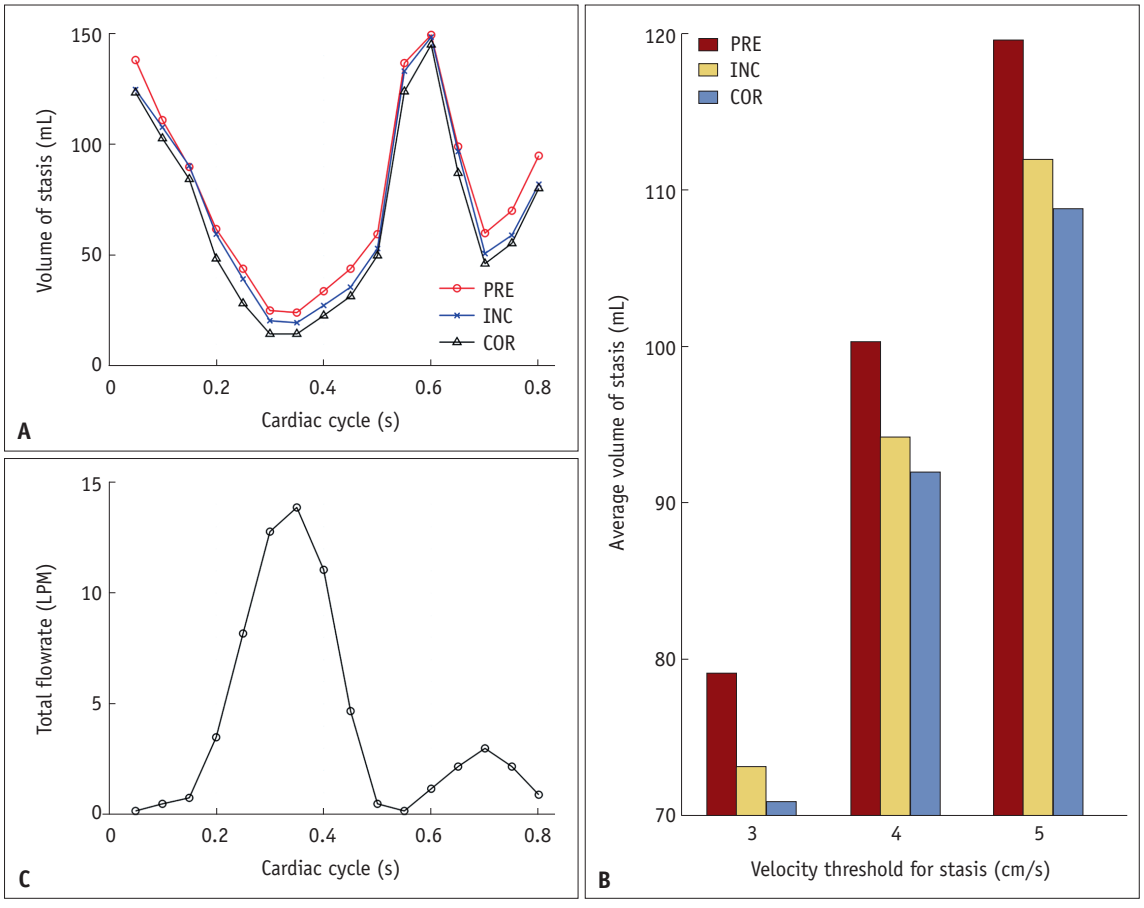

Fig. 5. Comparison of left atrium (LA) flow stasis among correctly occluded (COR), incorrectly occluded (INC), and pre-occlusion (PRE) LA phantoms. **A:** Volume of LA stasis ($|\vec{V}|$ < 3 cm/s) during a cardiac cycle. **B:** Average volume of stasis with different velocity thresholds ranging from 3–5 cm/s. **C:** The total flow rate variation during the cardiac cycle. LPM = liter per minute

https://doi.org/10.3348/kjr.2023.0173

Table 2. Comparison of Time-averaged Left Atrial Stasis Volume and Volume of Stasis with Respect to the Persistency of Stasis for the Three Phantoms

	Stasis Volume within the Entire LA Phantoms			Stasis Volume within the Common LA Chamber, Excluding Appendage*			Stasis Volume within the Remnant Appendage Pouch	
	COR	INC	PRE	COR	INC	PRE	INC†	PRE‡
Entire volume, mL	181.72	187.54	199.21	181.72	181.72	181.72	5.82	17.49
Time-averaged volume of LA stasis, mL	70.82 (39.0)	73.17 (39.0)	79.11 (39.7)	69.97 (38.5)	69.03 (38.0)	68.94 (37.9)	4.14 (71.2)	10.17 (58.2)
r_{stasis} > 40%, mL	58.58 (32.2)	63.49 (33.9)	68.10 (34.2)	57.99 (31.9)	58.69 (32.3)	57.43 (31.6)	4.80 (82.6)	10.67 (61.0)
r_{stasis} > 50%, mL	38.25 (21.1)	42.54 (22.6)	46.84 (23.5)	37.49 (20.6)	38.02 (20.9)	38.54 (21.2)	4.52 (77.7)	8.30 (47.5)
r_{stasis} > 60%, mL	33.45 (18.4)	34.64 (18.5)	41.66 (20.9)	31.99 (17.6)	32.27 (17.8)	33.99 (18.7)	2.37 (40.8)	7.67 (43.9)

*Volume A in Figure 1, †Volume B in Figure 1, ‡Volume B plus C in Figure 1. The percentage values in parentheses are the ratios of the defined volume to the corresponding entire volume (i.e., the first low). r_{stasis} = relative flow stasis, LA = left atrium, COR = correctly occluded, INC = incorrectly occluded, PRE = pre-occlusion

Table 3. The Internal Volume of Iso-particle Residence Time (PRT)-surface When the PRT was Set to the 5 Cardiac Cycles

	COR	INC	PRE
Entire volume, mL	181.72	187.54	199.21
Volume covered by iso-PRT-surface, mL	3.88 (2.1)	5.56 (3.0)	10.57 (5.3)

The percentage values in parentheses are the ratios of the defined volume to the corresponding entire volume (i.e., the first low). COR = correctly occluded, INC = incorrectly occluded, PRE = pre-occlusion

appendage area, no significant differences in the stasis volume was observed among the three phantoms. However, we found that the flow stasis volume and percentage within the LAA in the pre-occlusion model and remnant pouch in the incorrectly occluded model was substantially high (10.17 mL [58.2%] and 4.14 mL [71.2%], respectively).

Table 3 summarizes the internal volume of the iso-PRT surface at a PRT set to five cardiac cycles. Figure 6 shows a comparison of the iso-PRT surfaces. The blood particle volume, which took more than 5 cardiac cycles to leave the LA, was lowest in the correctly occluded model (3.88 mL; 2.14%), followed by the incorrectly occluded (5.56 mL; 2.96%) and pre-occlusion (10.57 mL; 5.31%) models.

ECAP

The Supplementary Figure 1 shows the distribution of TA|WSS|, OSI, and ECAP, as well as their area ratios to the segmented LA surface among the three LA phantoms. The lowest surface-and-time-averaged WSS was associated with the pre-occlusion model (0.048 Pa), followed by the incorrectly- (0.059 Pa) and correctly (0.072 Pa) occluded models. The surface-averaged OSI values were 0.148 and 0.149 for the incorrectly occluded and pre-occlusion models, respectively, which were slightly lower than those for the correctly occluded model (0.151). The surface-averaged ECAP was the highest in the pre-occlusion model (5.861 Pa^{-1}), followed by the incorrectly- (4.792 Pa^{-1}) and correctly (4.004 Pa^{-1}) occluded models (Fig. 7, Table 4).

DISCUSSION

In this experimental study, we directly visualized and compared different LA hemodynamics and flow metrics within three different 3D-printed LA models (pre-occlusion, incorrectly occluded, and correctly occluded LAAs), using 4D flow MRI. The correctly occluded model was associated with the lowest time-averaged stasis volume, internal iso-PRT surface volume, and ECAP and the highest surface-and-time-averaged WSS among the three models. This suggests that a correctly occluded LAA potentially leads to the greatest reduction in LA flow stasis and thrombogenicity in patients with AF.

Considering that the flow stasis volume and percentage within the common LA chamber (volume A in Fig. 2; middle column in Table 2) showed little difference among the three LA phantoms, it seems that LAAO did not significantly alter the flow stasis within the common LA chamber. The small portion of remaining LAA after incorrect occlusion (volume B in Fig. 2; the so-called remnant pouch) showed the highest percentage of flow stasis for all conditions except r_{stasis} > 60%, indicating that the remnant pouch may be a source of thrombus formation during the postprocedural follow-up period. Thus, operators should do their best to minimize or eliminate any remnants. These findings have clinical implications for achieving correct occlusion in routine LAAO cases. If a remnant pouch is found during

https://doi.org/10.3348/kjr.2023.0173

Korean Journal of Radiology
KJR

the procedure, the pouch should be adjusted. However, if correct occlusion cannot be achieved despite best efforts, or if a remnant pouch is found after the procedure due to conformational changes in the device associated with the complex interaction between the device and surrounding structures, the anticoagulant regimen can be modified and

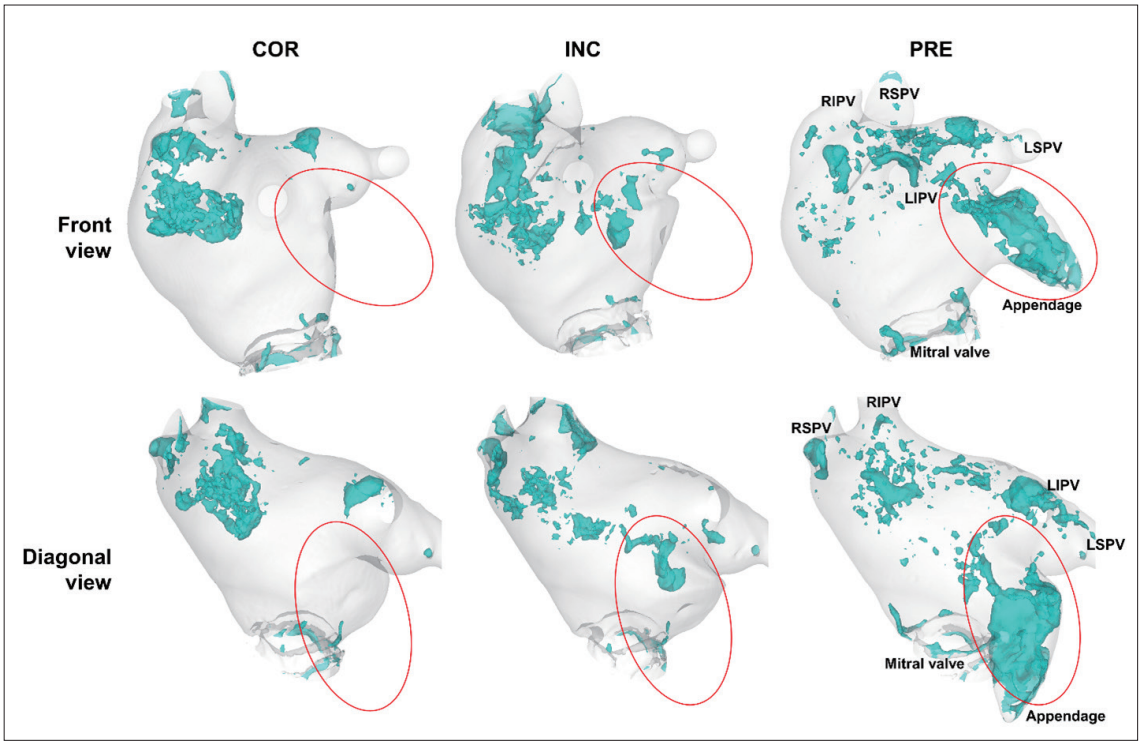

Fig. 6. Surfaces of the initial positions of fluid particles at a particle residence time (PRT) of 5 cardiac cycles (4 seconds) in correctly occluded (COR), incorrectly occluded (INC), and pre-occlusion (PRE) left atrium phantoms. The internal volume of the iso-PRT surface is the lowest in the COR model, followed by the INC and PRE models. The red circles indicate appendages and neighboring regions. RSPV = right superior pulmonary vein, RIPV = right inferior pulmonary vein, LIPV = left inferior pulmonary vein, LSPV = left superior pulmonary vein

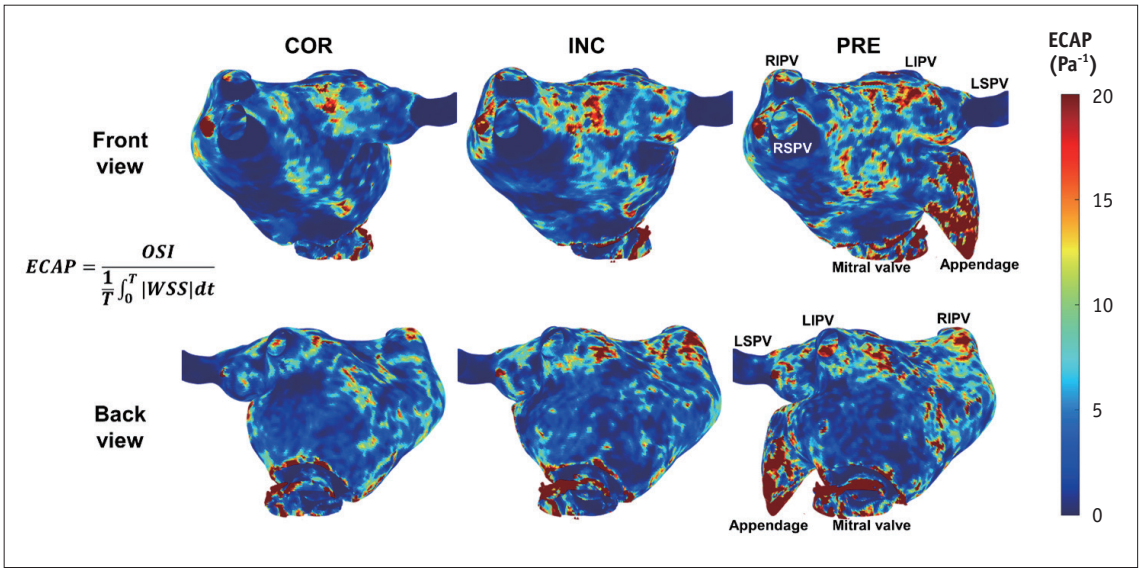

Fig. 7. Endothelial cell activation potential contours in the front and back projections of the 3D structures of correctly occluded (COR), incorrectly occluded (INC), and pre-occlusion (PRE) left atrium phantoms. Surface-averaged endothelial cell activation potential (ECAP) is lowest for COR and highest for PRE. OSI = oscillatory shear index, WSS = wall shear stress, RSPV = right superior pulmonary vein, RIPV = right inferior pulmonary vein, LIPV = left inferior pulmonary vein, LSPV = left superior pulmonary vein

https://doi.org/10.3348/kjr.2023.0173

Table 4. Comparison of STA|WSS|, Surface-averaged OSI, and Surface-averaged ECAP Among Pre-occlusion (PRE), Incorrectly Occluded (INC), and Correctly Occluded (COR) Phantoms

	COR	INC	PRE
STA|WSS| (Pa)	0.072	0.059	0.048
Surface-averaged OSI	0.151	0.148	0.149
Surface-averaged ECAP (Pa^{-1})	4.004	4.792	5.861

STA|WSS| = surface-and-time-averaged wall shear stress, OSI = oscillatory shear index, ECAP = endothelial cell activation potential

optimized based on the integrated thrombotic burden of the patient. An individualized approach based on post-procedure hemodynamic results as well as clinical risk factors and situations may improve treatment outcomes by reducing the risk of ischemic stroke or bleeding events. The establishment of an antithrombotic treatment strategy based on the final post-procedure hemodynamic results as well as clinical risk factors and situations is ideal (Fig. 1).

Several studies have utilized 4D flow MRI to assess flow patterns in patients with AF. Markl et al. [25] have demonstrated that 4D flow MRI can detect changes in global and regional LA flow dynamics, such as stasis and peak velocities, in patients with AF. Demirkiran et al. [26] have also revealed that 4D flow MRI-driven LA dynamics, including velocity, stasis fraction, and kinetic energy, were impaired in patients with paroxysmal AF compared with the control group. Garcia et al. [16] have demonstrated that the LA vortex size obtained via 4D flow MRI was associated with the thromboembolic risk in patients with paroxysmal AF. However, most previous studies have compared LA and LAA flow dynamics of patients with AF with those of healthy controls. Although our study was in vitro in nature, one of the major developments in our study was that postprocedural flow changes were assessed and compared using 4D flow MRI. Additionally, we focused on the LAA and the remnant pouch—the main sources of thrombogenicity—and their hemodynamic interaction with the LA, along with the implications of the results on treatment.

With technical advancements in image acquisition and analysis for 4D flow MRI, various hemodynamic parameters have been developed and utilized. In the present study, we analyzed thrombogenesis-related quantitative hemodynamic parameters, such as time-averaged WSS, OSI, and ECAP [24,27-32]. WSS, defined as the frictional shear stress on the cardiovascular wall, is highly involved in thrombus formation. A low WSS promotes the stasis of blood flow, leading to the accumulation of blood cells and fibrin, and therefore, the progression of a thrombus. In contrast, a high WSS can cause endothelial cell damage, exposing the subendothelial matrix and triggering platelet activation and thrombus formation [33,34]. OSI, which refers to the change in the direction of the WSS vector during the cardiac cycle, is strongly associated with disturbances in blood flow patterns. A high OSI can cause endothelial cell dysfunction due to vortex formation and flow stasis, leading to thrombus progression [35]. ECAP, defined as the ratio of OSI to TA|WSS|, has been proposed as an index for identifying areas where endothelial cells are activated in response to blood flow and are likely to promote inflammation [24,30]. This is the first study to visualize and quantify posttreatment hemodynamic outcomes by demonstrating a stepwise decrease in stagnant volume, time, and ECAP depending on the degree of occlusion ($ECAP_{pre\text{-}occlusion}$ > $ECAP_{incorrect\ occlusion}$ > $ECAP_{correct\ occlusion}$). Although LAAO has been adopted as an alternative option for the prevention of thromboembolic events in patients intolerant of long-term OAC, its clinical benefit has primarily been driven by reduced bleeding events rather than ischemic stroke or thromboembolic events [36,37]. Our results provide concrete evidence that LAAO improves LA flow dynamics and reduces thromboembolic risk.

Due to the complex anatomical variations of LAAs, such as in branching and angulation, occluders with a plug-like design cannot always fit all types and sizes of LAAs. However, most randomized trials have adopted plug-like closure devices. Consequently, correct occlusion may not be achieved in all cases. This may be one of the reasons why these studies did not show significantly reduced thrombotic events with surgically performed LAA exclusion, as demonstrated in the LAAOS III trial [38]. Current risk stratification schemes used to guide clinical decisions are dependent on clinical risk factors that do not fully reflect the hemodynamic state of patients with AF. Through treatment decisions that reflect both the clinical risk and hemodynamic state, treatment efficacy and potential clinical benefits can be maximized.

Our study has several limitations. First, the experiments were performed based on the clinical and imaging findings of a single patient. Therefore, the generalizability of the results may be limited. Second, the LA phantoms were made of rigid plastic resin; therefore, the elasticity and contractility of the LA wall was not reflected in the phantom models. Nevertheless, as patients with long-standing persistent AF have minimal phasic variations in LA volume, errors due to neglecting LA elasticity and contractility seem to be minimal. In addition, previous studies have shown that

https://doi.org/10.3348/kjr.2023.0173

Korean Journal of Radiology
KJR

4D flow MRI studies using rigid cardiovascular phantoms and computational fluid dynamics studies based on fixed boundary assumptions enable reliable validation of in vivo results [39-42]. Third, there are limitations in the flow simulation. The left ventricular diastolic suction and detailed mitral valve physiology associated with the left ventricle and its apparatus could not be simulated, and the irregular cardiac cycle length accompanying AF variations was replaced with a uniform pulmonary venous pulsation at a constant heart rate. Nevertheless, this experimental study has several strengths. In vitro phantom studies are relatively free from scan time limitations and metal-related artifacts; thus, higher temporal and spatial resolutions and more accurate flow metrics were available in this study. Additionally, the effects of the LAAO and occluder position could be purposefully evaluated in isolation, as other variables in the experiments were fixed. The primary goal of this study was to broaden the clinical understanding of LAAO based on detailed and quantitative MRI data. Further in vivo 4D flow MR studies with larger study populations will be conducted.

In conclusion, our experiments showed that correctly occluded LAAs can lead to the greatest reduction in LA flow stasis and thrombogenicity, presenting a tentative procedural goal to maximize clinical benefits in patients with AF. Further in vivo investigations with larger numbers of patients are warranted to examine these findings under actual physiological conditions.

Supplement

The Supplement is available with this article at https://doi.org/10.3348/kjr.2023.0173.

Supplementary Video Legends

Video 1. 4D flow magnetic resonance imaging for the visualization of the flow components within the left atrium (LA) phantoms at peak pulmonary venous flow using the particle tracing technique. The distribution, orientation, and magnitude of the flow differed among the three LA phantoms. COR = correctly occluded, INC = incorrectly occluded, PRE = pre-occlusion

Availability of Data and Material

The datasets generated or analyzed during the study are available from the corresponding author on reasonable request.

Conflicts of Interest

The authors have no potential conflicts of interest to disclose.

Author Contributions

Conceptualization: Seung Yong Shin, Simon Song. Data curation: Min Jae Cha, Don-Gwan An. Formal analysis: Don-Gwan An, Minsoo Kang. Funding acquisition: Min Jae Cha, Simon Song. Investigation: Min Jae Cha, Don-Gwan An, Hyue Mee Kim, Iksung Cho, Hyewon Choi. Methodology: Min Jae Cha, Don-Gwan An, Seung Yong Shin, Simon Song. Project administration: Simon Song. Resources: Joonhwa Hong, Jee-Hyun Cho, Simon Song. Software: Don-Gwan An, Minsoo Kang. Supervision: Sang-Wook Kim, Seung Yong Shin, Simon Song. Validation: Min Jae Cha, Don-Gwan An, Seung Yong Shin, Simon Song. Visualization: Don-Gwan An. Writing—original draft: Min Jae Cha, Don-Gwan An, Seung Yong Shin, Simon Song.

ORCID iDs

Min Jae Cha
https://orcid.org/0000-0001-6358-8081
Don-Gwan An
https://orcid.org/0000-0003-0958-2361
Minsoo Kang
https://orcid.org/0000-0001-5733-1255
Hyue Mee Kim
https://orcid.org/0000-0001-7680-6690
Sang-Wook Kim
https://orcid.org/0000-0002-7208-8596
Iksung Cho
https://orcid.org/0000-0001-5927-5410
Joonhwa Hong
https://orcid.org/0000-0003-2212-2861
Hyewon Choi
https://orcid.org/0000-0003-3735-6791
Jee-Hyun Cho
https://orcid.org/0000-0002-0140-9188
Seung Yong Shin
https://orcid.org/0000-0002-3408-6899
Simon Song
https://orcid.org/0000-0002-4043-9443

Funding Statement

This research was supported by the Chung-Ang University Research Grants in 2019 and the National Research Foundation of Korea (NRF) grant funded by the Korea

government (Ministry of Science, ICT, and Future Planning) (No. 2021R1A2B5B03002103 and 2022R1A5A1022977).

Acknowledgments

The authors appreciate the technical assistance of Mun Young Paek (from Siemens Healthcare), Bon Chul Ha, Hyeong Ho So and Min Gu Kim for helping with MRI scans.

REFERENCES

1. Pellman J, Sheikh F. Atrial fibrillation: mechanisms, therapeutics, and future directions. *Compr Physiol* 2015;5:649-665
2. Go AS, Hylek EM, Phillips KA, Chang Y, Henault LE, Selby JV, et al. Prevalence of diagnosed atrial fibrillation in adults: national implications for rhythm management and stroke prevention: the AnTicoagulation and Risk Factors in Atrial Fibrillation (ATRIA) Study. *JAMA* 2001;285:2370-2375
3. Holmes DR Jr, Lakkireddy DR, Whitlock RP, Waksman R, Mack MJ. Left atrial appendage occlusion: opportunities and challenges. *J Am Coll Cardiol* 2014;63:291-298
4. Kirchhof P, Benussi S, Kotecha D, Ahlsson A, Atar D, Casadei B, et al. 2016 ESC Guidelines for the management of atrial fibrillation developed in collaboration with EACTS. *Eur Heart J* 2016;37:2893-2962
5. Blackshear JL, Odell JA. Appendage obliteration to reduce stroke in cardiac surgical patients with atrial fibrillation. *Ann Thorac Surg* 1996;61:755-759
6. Saw J, Lempereur M. Percutaneous left atrial appendage closure: procedural techniques and outcomes. *JACC Cardiovasc Interv* 2014;7:1205-1220
7. Holmes DR, Reddy VY, Turi ZG, Doshi SK, Sievert H, Buchbinder M, et al. Percutaneous closure of the left atrial appendage versus warfarin therapy for prevention of stroke in patients with atrial fibrillation: a randomised non-inferiority trial. *Lancet* 2009;374:534-542
8. Holmes DR Jr, Kar S, Price MJ, Whisenant B, Sievert H, Doshi SK, et al. Prospective randomized evaluation of the Watchman Left Atrial Appendage Closure device in patients with atrial fibrillation versus long-term warfarin therapy: the PREVAIL trial. *J Am Coll Cardiol* 2014;64:1-12
9. Osmancik P, Herman D, Neuzil P, Hala P, Taborsky M, Kala P, et al. Left atrial appendage closure versus direct oral anticoagulants in high-risk patients with atrial fibrillation. *J Am Coll Cardiol* 2020;75:3122-3135
10. Staubach S, Schlatterbeck L, Mörtl M, Strohm H, Hoppmann P, Laugwitz KL, et al. Long-term transesophageal echocardiography follow-up after percutaneous left atrial appendage closure. *Heart Rhythm* 2020;17(5 Pt A):728-733
11. Mohanty S, Gianni C, Trivedi C, Gadiyaram V, Della Rocca DG, MacDonald B, et al. Risk of thromboembolic events after percutaneous left atrial appendage ligation in patients with atrial fibrillation: long-term results of a multicenter study. *Heart Rhythm* 2020;17:175-181
12. Asinger RW, Koehler J, Pearce LA, Zabalgoitia M, Blackshear JL, Fenster PE, et al. Pathophysiologic correlates of thromboembolism in nonvalvular atrial fibrillation: II. Dense spontaneous echocardiographic contrast (The Stroke Prevention in Atrial Fibrillation [SPAF-III] study). *J Am Soc Echocardiogr* 1999;12:1088-1096
13. Markl M, Lee DC, Ng J, Carr M, Carr J, Goldberger JJ. Left atrial 4-dimensional flow magnetic resonance imaging: stasis and velocity mapping in patients with atrial fibrillation. *Invest Radiol* 2016;51:147-154
14. Markl M, Lee DC, Furiasse N, Carr M, Foucar C, Ng J, et al. Left atrial and left atrial appendage 4D blood flow dynamics in atrial fibrillation. *Circ Cardiovasc Imaging* 2016;9:e004984
15. Markl M, Fluckiger J, Lee DC, Ng J, Goldberger JJ. Velocity quantification by electrocardiography-gated phase contrast magnetic resonance imaging in patients with cardiac arrhythmia: a simulation study based on real time transesophageal echocardiography data in atrial fibrillation. *J Comput Assist Tomogr* 2015;39:422-427
16. Garcia J, Sheitt H, Bristow MS, Lydell C, Howarth AG, Heydari B, et al. Left atrial vortex size and velocity distributions by 4D flow MRI in patients with paroxysmal atrial fibrillation: associations with age and CHA(2) DS(2) -VASc risk score. *J Magn Reson Imaging* 2020;51:871-884
17. Elkins C, Markl M, Iyengar A, Wicker R, Eaton JK. Full-field velocity and temperature measurements using magnetic resonance imaging in turbulent complex internal flows. *Int J Heat Fluid Flow* 2004;25:702-710
18. Benson MJ, Banko AJ, Elkins CJ, An DG, Song S, Bruschewski M, et al. The 2019 MRV challenge: turbulent flow through a U-bend. *Exp Fluids* 2020;61:148
19. Wang CY, Gao Q, Wang HP, Wei RJ, Li T, Wang JJ. Divergence-free smoothing for volumetric PIV data. *Exp Fluids* 2016;57:15
20. Bluestein D, Niu L, Schoephoerster RT, Dewanjee MK. Steady flow in an aneurysm model: correlation between fluid dynamics and blood platelet deposition. *J Biomech Eng* 1996;118:280-286
21. Rayz VL, Boussel L, Lawton MT, Acevedo-Bolton G, Ge L, Young WL, et al. Numerical modeling of the flow in intracranial aneurysms: prediction of regions prone to thrombus formation. *Ann Biomed Eng* 2008;36:1793-1804
22. Ko S, Yang B, Cho JH, Lee J, Song S. Novel and facile criterion to assess the accuracy of WSS estimation by 4D flow MRI. *Med Image Anal* 2019;53:95-103
23. Yang B, Cho JH, Lee J, Song S. Development of custom-made RF coil for magnetic resonance velocimeter with a high spatial resolution. *J Mech Sci Technol* 2019;33:1681-1688
24. Di Achille P, Tellides G, Figueroa CA, Humphrey JD. A haemodynamic predictor of intraluminal thrombus formation in abdominal aortic aneurysms. *Proc R Soc A* 2014;470:20140163
25. Markl M, Carr M, Ng J, Lee DC, Jarvis K, Carr J, et al. Assessment of left and right atrial 3D hemodynamics in patients with atrial fibrillation: a 4D flow MRI study. *Int J*

https://doi.org/10.3348/kjr.2023.0173

Cardiovasc Imaging 2016;32:807-815
26. Demirkiran A, Amier RP, Hofman MBM, van der Geest RJ, Robbers LFHJ, Hopman LHGA, et al. Altered left atrial 4D flow characteristics in patients with paroxysmal atrial fibrillation in the absence of apparent remodeling. *Sci Rep* 2021;11:5965
27. Zambrano BA, Gharahi H, Lim C, Jaberi FA, Choi J, Lee W, et al. Association of intraluminal thrombus, hemodynamic forces, and abdominal aortic aneurysm expansion using longitudinal CT images. *Ann Biomed Eng* 2016;44:1502-1514
28. Kelsey LJ, Powell JT, Norman PE, Miller K, Doyle BJ. A comparison of hemodynamic metrics and intraluminal thrombus burden in a common iliac artery aneurysm. *Int J Numer Method Biomed Eng* 2017;33:e2821
29. Ong C, Xiong F, Kabinejadian F, Praveen Kumar G, Cui F, Chen G, et al. Hemodynamic analysis of a novel stent graft design with slit perforations in thoracic aortic aneurysm. *J Biomech* 2019;85:210-217
30. Kandail H, Hamady M, Xu XY. Effect of a flared renal stent on the performance of fenestrated stent-grafts at rest and exercise conditions. *J Endovasc Ther* 2016;23:809-820
31. Ku DN, Giddens DP, Zarins CK, Glagov S. Pulsatile flow and atherosclerosis in the human carotid bifurcation. Positive correlation between plaque location and low oscillating shear stress. *Arteriosclerosis* 1985;5:293-302
32. Markl M, Frydrychowicz A, Kozerke S, Hope M, Wieben O. 4D flow MRI. *J Magn Reson Imaging* 2012;36:1015-1036
33. Fukumoto Y, Hiro T, Fujii T, Hashimoto G, Fujimura T, Yamada J, et al. Localized elevation of shear stress is related to coronary plaque rupture: a 3-dimensional intravascular ultrasound study with in-vivo color mapping of shear stress distribution. *J Am Coll Cardiol* 2008;51:645-650
34. Chatzizisis YS, Jonas M, Coskun AU, Beigel R, Stone BV, Maynard C, et al. Prediction of the localization of high-risk coronary atherosclerotic plaques on the basis of low endothelial shear stress: an intravascular ultrasound and histopathology natural history study. *Circulation* 2008;117:993-1002
35. Hwang J, Saha A, Boo YC, Sorescu GP, McNally JS, Holland SM, et al. Oscillatory shear stress stimulates endothelial production of O2- from p47phox-dependent NAD(P)H oxidases, leading to monocyte adhesion. *J Biol Chem* 2003;278:47291-47298
36. Briceno DF, Villablanca P, Cyrille N, Massera D, Bader E, Manheimer E, et al. Left atrial appendage occlusion device and novel oral anticoagulants versus warfarin for stroke prevention in nonvalvular atrial fibrillation: systematic review and meta-analysis of randomized controlled trials. *Circ Arrhythm Electrophysiol* 2015;8:1057-1064
37. Holmes DR Jr, Alkhouli M, Reddy V. Left atrial appendage occlusion for the unmet clinical needs of stroke prevention in nonvalvular atrial fibrillation. *Mayo Clin Proc* 2019;94:864-874
38. Whitlock RP, Belley-Cote EP, Paparella D, Healey JS, Brady K, Sharma M, et al. Left atrial appendage occlusion during cardiac surgery to prevent stroke. *N Engl J Med* 2021;384:2081-2091
39. Ha H, Huh HK, Park KJ, Dyverfeldt P, Ebbers T, Kim DH, et al. In-vitro and In-vivo assessment of 4D flow MRI reynolds stress mapping for pulsatile blood flow. *Front Bioeng Biotechnol* 2021;9:774954
40. Biglino G, Cosentino D, Steeden JA, De Nova L, Castelli M, Ntsinjana H, et al. Using 4D cardiovascular magnetic resonance imaging to validate computational fluid dynamics: a case study. *Front Pediatr* 2015;3:107
41. Toger J, Bidhult S, Revstedt J, Carlsson M, Arheden H, Heiberg E. Independent validation of four-dimensional flow MR velocities and vortex ring volume using particle imaging velocimetry and planar laser-Induced fluorescence. *Magn Reson Med* 2016;75:1064-1075
42. Habigt MA, Gesenhues J, Stemmler M, Hein M, Rossaint R, Mechelinck M, et al. In vivo validation of a cardiovascular simulation model in pigs. *Math Comput Appl* 2022;27:28

 https://doi.org/10.3348/kjr.2023.0173